Research article

Vincenzo Caligiuri*, Milan Palei, Giulia Biffi and Roman Krahne*

Hybridization of epsilon-near-zero modes via resonant tunneling in layered metal-insulator double nanocavities

Abstract: The coupling between multiple nanocavities in close vicinity leads to the hybridization of their modes. Stacked metal-insulator-metal (MIM) nanocavities constitute a highly versatile and very interesting model system to study and engineer such mode coupling, as they can be realized by lithography-free fabrication methods with fine control on the optical and geometrical parameters. The resonant modes of such MIM cavities are epsilon-near-zero (ENZ) resonances, which are appealing for non-linear photophysics and a variety of applications. Here, we study the hybridization of ENZ resonances in MIMIM nanocavities, obtaining a very large mode splitting reaching 0.477 eV, Q-factors of the order of 40 in the visible spectral range, and fine control on the resonance wavelength and mode linewidth by tuning the thickness of the dielectric and metallic layers. A semiclassical approach that analyzes the MIMIM structure as a double quantum well system allows to derive the exact analytical dispersion relation of the ENZ resonances, achieving perfect agreement with numerical simulations and experiments. Interestingly, the asymmetry of the mode splitting in a symmetric MIMIM cavity is not reflected in the classical model of coupled oscillators, which can be directly related to quantum mechanical tunneling for the coupling of the two cavities. Interpreting the cavity resonances as resonant tunneling modes elucidates that they can be excited without momentum matching techniques. The broad tunability of high-quality ENZ resonances together with their

strong coupling efficiency makes such MIMIM cavities an ideal platform for exploring light-matter interaction, for example, by the integration of quantum emitters in dielectric layers.

1 Introduction

The design of photonic nanocavities with tunable resonance wavelengths is of fundamental interest for many purposes in optics. Among the important aspects for such nanocavities are their ease of integration with other photonic elements [1], the quality factor [2, 3] and tunability range of the resonance [3, 4], and the cavity losses [5–7]. Plasmonic nanocavities have the advantage of strong subwavelength light confinement and resonance tunability [8]. However, high-quality factors are difficult to achieve [9], intrinsic losses caused by the metals set a limit for light amplification, and possibly the integration with other systems is highly demanding due to the elaborate three-dimensional shapes of the plasmonic resonators. In this respect, nanocavities with epsilon-near-zero (ENZ) resonances are a promising alternative, as in this case the imaginary part of the effective dielectric permittivity at their resonances is small [5], and ENZ nanocavities with possibly multiple tunable resonances with high-quality factor could constitute a promising alternative as photonic resonators. Toward such tunable cavities, the coupling of resonators provides a viable approach that enables to tailor the optical response, as coupled resonators manifest a splitting of their resonant modes [10–13].

Planar photonic nanocavities made of metal-insulator-metal (MIM) layers constitute a versatile platform for engineering nanocavities with strong light confinement in a broad frequency range [1, 6, 14–26], and the possibility of fabricating vertically stacked systems

Corresponding authors: Vincenzo Caligiuri and Roman Krahne, Istituto Italiano di Tecnologia, Via Morego 30, 16163 Genova, Italy, e-mail: vincenzo.caligiuri@iit.it (V. Caligiuri); roman.krahne@iit.it (R. Krahne). https://orcid.org/0000-0003-0066-7019 (R. Krahne)
Milan Palei and Giulia Biffi: Istituto Italiano di Tecnologia, Via Morego 30, 16163 Genova, Italy; and Dipartimento di Chimica e Chimica Industriale, Università degli Studi di Genova, Via Dodecaneso, 31, 16146 Genova, Italy

allows for the design of coupled resonators [8]. Furthermore, their ease in fabrication, together with the broad variety of employable materials, makes MIM cavities an ideal system for the exploration of nonlinear optical properties [11, 27, 28]. The effective dielectric permittivity of MIM nanoresonators can be designed to manifest very high positive or negative values (eventually showing a pole) [27, 29, 30], or to completely vanish, manifesting ENZ behavior if losses are sufficiently small [31–34]. Such ENZ resonances have been referred to as "Ferrell-Berreman" modes because of the similarity to the zero crossing of the dielectric permittivity in plasmon-polaritonic and phonon-polaritonic thin films [5, 35–38]. However, for few-layer metal/insulator stacks, the origin and nature of the ENZ resonances are still under investigation [5, 7, 39]. For example, the effective medium theory fails to predict their effective permittivity [5, 40, 41], and it can be debated if the ENZ resonances are photonic or plasmonic or if classical or quantum mechanical models should be applied [7]. In a recent work, we demonstrated that MIM cavities can be seen as a double barrier quantum well and that the ENZ cavity modes can be treated as the resonant tunneling of photons [7]. Furthermore, the occurrence of an ENZ frequency in the permittivity is usually accompanied by an increase of the local density of photonic states [32, 33], which can be exploited for the enhancement of the radiative rate of, for example, a perovskite nanocrystal film deposited on the surface of an MIMIM structure [5].

In this paper, we study the mode splitting of the resonances in layered MIMIM double nanocavities. We demonstrate the ENZ nature of the resonant modes by spectroscopic ellipsometry and map the anticrossing of the modes by detuning the resonance frequency of one cavity through variation of the thickness of one dielectric layer. We show that the coupling strength that governs the mode splitting can be finely tuned via the thickness of the central metal layer, and we demonstrate that the linewidth of the resonances can be optimized by acting on the thickness of the outer metal films. To gain deeper insight into the optical properties of such MIMIM cavities, we present a semiclassical analysis of their resonant modes, which demonstrates that the MIMIM cavity can be viewed as a double quantum well. The symmetric and antisymmetric resonances occurring at lower and higher energy, respectively, represent the typical two-level system as it is successfully described in quantum mechanics, with the ammonia molecule as a prominent example. In particular, the MIMIM system manifests an asymmetric mode splitting, which is characteristic for quantum mechanical coupling that is nonlinear, in contrast to the classical system where oscillators are linearly coupled [10]. Other advantages of the double quantum well model for the MIMIM structure lie in the analytical solutions for the resonance frequencies and the fact that it directly elucidates why the cavity resonances can be excited by illumination from the top, through the metal layers, without the need of a momentum matching technique. We note that the system that we address in this work is different from the one discussed by Alaeian and Dionne [8], as they treat plasmonic modes in MIMIM structures with much thinner dielectric layers that do not correspond to ENZ resonances.

2 Results and discussion

The structure of an experimentally fabricated MIMIM double cavity consisting of silver (Ag) as metal and Al_2O_3 as insulator (dielectric) is sketched in Figure 1A. Here, the dielectric cavity layers have nearly similar thickness of 100 and 115 nm, and the three metal layers of Ag were chosen with a thickness of 20 nm. Such a double cavity manifests two distinct peaks in absorbance and transmittance, and two corresponding minima in reflectance that occur at 470 and 610 nm, and which can be associated to the high- and low-energy cavity modes (Figure 1B). The real (ε') and imaginary (ε'') parts of the ellipsometrically measured dielectric permittivity are depicted Figure 1C and D, respectively. The curve of ε' crosses the zero at four wavelengths, two of which ($\omega_{\text{HE-ENZ}}$ and $\omega_{\text{LE-ENZ}}$) are characterized by a small imaginary part, which renders them high-quality ENZ modes. Such ENZ resonances correspond to Ferrell-Berreman modes that occur naturally in thin Ag films (at 327 nm) and that can be designed within certain spectral bands in layered metamaterials [5, 38]. Interestingly, the wavelengths of these ENZ modes coincide with the cavity features in the optical spectra in Figure 1B, as highlighted by the vertical dashed lines, which indicates that the cavity modes of the MIMIM correspond to ENZ resonances. For an analytical modeling of the effective dielectric permittivity of the MIMIM structure, we extended the harmonic oscillator model that we developed for a single MIM system in Ref. [5]. Then, the double cavity system can be described by adding two damped oscillator terms, one for each MIM, to the Drude expression of the dielectric permittivity of Ag:

$$\varepsilon_{\text{eff,MIMIM(Ag)}} = \varepsilon_{\infty} - \frac{\omega_{\text{p}}^2}{(\omega^2 + i\gamma\omega)} - \frac{\alpha_1 \omega_{\text{MIM}}^2}{(\omega^2 - \omega_{0,\text{MIM1}}^2 + i\gamma_{\text{MIM1}}\omega)}$$
$$- \frac{\alpha_2 \omega_{\text{MIM}}^2}{(\omega^2 - \omega_{0,\text{MIM2}}^2 + i\gamma_{\text{MIM2}}\omega)}; \tag{1}$$
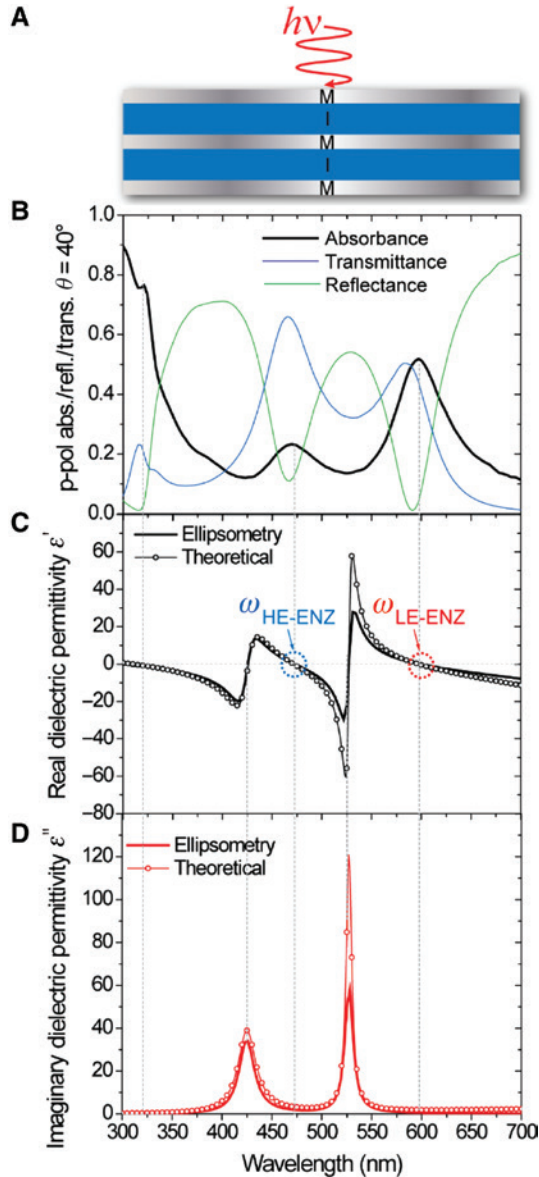
Figure 1: Optical properties of the MIMIM structure.
(A) Architecture of the MIMIM structure with illumination from the top. (B) Ellipsometrically measured p-polarized transmittance (blue), reflectance (green), and absorbance (black), detected at $\theta = 40°$, showing two absorbance maxima at the two low-loss ENZ wavelengths. (C and D) Theoretically modeled (empty circles) and ellipsometrically measured (solid line) real (C) and imaginary (D) effective dielectric permittivity of an MIMIM cavity. Low-loss ENZ wavelengths are highlighted with blue (high-energy) and red (low-energy) dashed circles.

Here, $\gamma_{Ag} = 0.021$ eV and $\omega_p = 9.1$ eV are the Drude parameters of Ag. ε_∞ is taken as a fitting parameter, and we obtain $\varepsilon_\infty = 6.8$, which is slightly larger than the value of Ag due to the residual polarizability of the system. The parameters $\omega_{0,MIM1} = 2.452$ eV, $\omega_{0,MIM2} = 2.7382$ eV, $\gamma_{MIM1} = 0.075$ eV, and $\gamma_{MIM2} = 0.07$ eV are obtained from the experimental

ellipsometry spectra. Moreover, it is convenient to fix the parameter ω_{MIM}^2 (at 3.53 eV) and to express the difference between the two oscillators in the numerator by a coefficient α_i (where i is the ith resonance). In this case, $\alpha_1 = 0.35$ and $\alpha_2 = 0.3$. The fitting with this approach is depicted by the open circles in Figure 1C and D and shows very good agreement with the experimental data. We note that Eq. (1) allows to describe the MIMIM system as one homogenized layer with an effective dielectric permittivity.

The modeling of the norm of the electric field with finite-element methods (COMSOL) at the resonance wavelengths shows that the cavity modes are strongly confined in the dielectric layers, as demonstrated in Figure S1 in the Supporting Information (SI).

The MIMIM double cavity can be seen as two MIM cavities stacked on top of each other that are connected by the central metal layer. This configuration resembles two coupled oscillators that lead to a mode splitting when the individual resonance frequencies are similar or only slightly detuned. In the case of MIM and MIMIM cavities, the resonance frequencies are mainly determined by the thickness of the dielectric layers; therefore, we can control the detuning in MIMIM cavities by varying the thickness of one dielectric layer while keeping the other one fixed.

Figure 2A shows the absorbance maxima of the high-energy (blue stars) and low-energy (red stars) resonances for five samples, where the bottom dielectric layer thickness varied from 60 to 160 nm, whereas that of the top layer was constant at 112 nm. We clearly observe the anticrossing behavior that is expected for two coupled modes, corroborated by scattering matrix method (SMM) simulations (dashed lines) [27, 42, 43]. A careful inspection of the experimental and simulated frequencies in the anticrossing region reveals that the shift of the high-energy (HE-ENZ) mode from the unperturbed frequency (solid gray line) is larger than that of the low-energy (LE-ENZ) mode. Such behavior deviates from the classical coupled oscillator model where a symmetric mode splitting occurs. The corresponding spectra are shown in Figure 2B, where we notice that the resonance associated to the top layer manifests a more pronounced absorbance peak outside the strong anticrossing region. The coupling strength of the ENZ modes is determined by the thickness of the central metal layer, as evident in Figure 2C. Here, symmetric MIMIM cavities were fabricated with fixed dielectric and outer metal layer thicknesses, whereas the thickness of the central Ag layer varied from 20 to 100 nm. Clearly, the mode splitting decreases with increasing central layer thickness. The anticrossing behavior of MIMIM structures with different mode splitting is shown in Figure S2 in the SI. Another important factor for photonic cavities is the quality of the resonances in

terms of linewidth and quality (Q) factor, where the latter is evaluated as the ratio of the full-width at half-maximum over central resonance frequency. In the black spectrum in Figure 2C, we obtain a Q-factor of 35 at 540 nm (2.3 eV) with a linewidth of 80 meV. However, such a performance
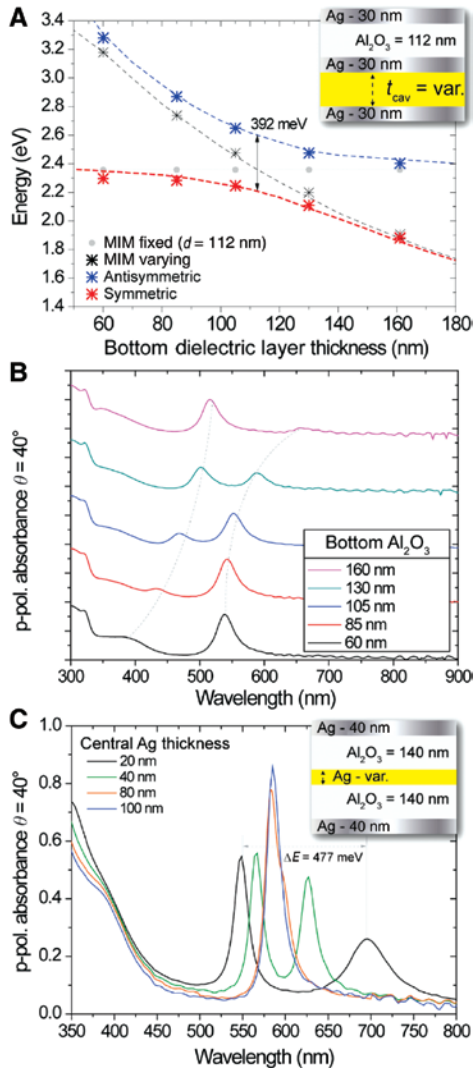
can be noticeably improved by acting on the thickness of the external metal layers. The SMM calculations in Figure 3 demonstrate that the quality of the resonances is mainly determined by the thickness of the outer metal layers, whereas the mode splitting, as determined by the central layer thickness, remains roughly constant. ENZ resonances with linewidth as low as 25 meV are achievable, together with very high Q-factors of about 100 (Figure 4B) that correspond to plasmon relaxation times of the order of 200 fs.

The MIMIM structure is therefore a highly versatile photonic cavity, where the frequency of the resonance modes, their quality factor, and the mode splitting can be tailored to a very large degree throughout the visible and near-infrared spectral range. In particular, the spectral range of the resonances can be extended by an adequate choice of the dielectric material, as demonstrated in Figure S3 where the resonances for MIMIM cavities with TiO_2 and SiO_2 are shown. Interestingly, for TiO_2 also the asymmetric resonances manifest hybridization and mode splitting. Therefore, MIMIM double cavities are appealing when the spectral overlap with dyes, quantum emitters, and other photonic systems is sought.

Motivated by the discrepancies of the optical properties of the MIMIM double cavity with the classical analytical model, we outline its analogy to a double quantum
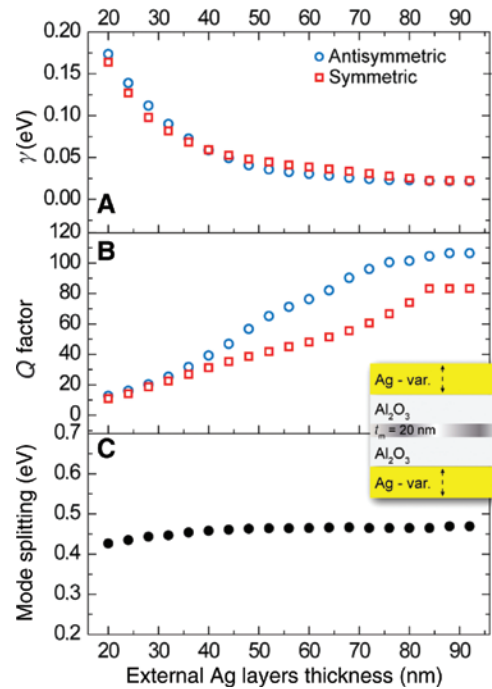

Figure 2: Mode splitting in a MIMIM double cavity.
(A) Mode anticrossing in a MIMIM system with 30 nm Ag layers and 112 nm Al_2O_3 as top dielectric layer, whereas the thickness of the bottom dielectric layer is varied. Experimentally measured data is shown by stars and the simulated dispersion via SMM is shown by dashed lines. The gray markers (experimental) and lines (SMM simulations) show the case of noninteracting cavities. (B) Absorbance spectra measured in p-polarization and obtained as (1-transmittance-reflectance) for the five MIMIM structures with different dielectric bottom layer thickness displayed in (A). (C) Ellipsometrically measured p-polarized absorbance curves for different thickness of the central layer. For a MIMIM with 20 nm central Ag layer, we obtained a mode splitting of 447 meV that corresponds to about six times the linewidth of the antisymmetric mode (see also Figure S2 in the SI for MIMIM systems with other metal layer thicknesses).

Figure 3: Dependence of the cavity resonances on the thickness of the external Ag layers.
SMM simulations of the (A) linewidth, (B) quality factor, and (C) mode splitting of a MIMIM system with 20 nm thickness of the central metal layer as a function of the thickness of the external metal layers.
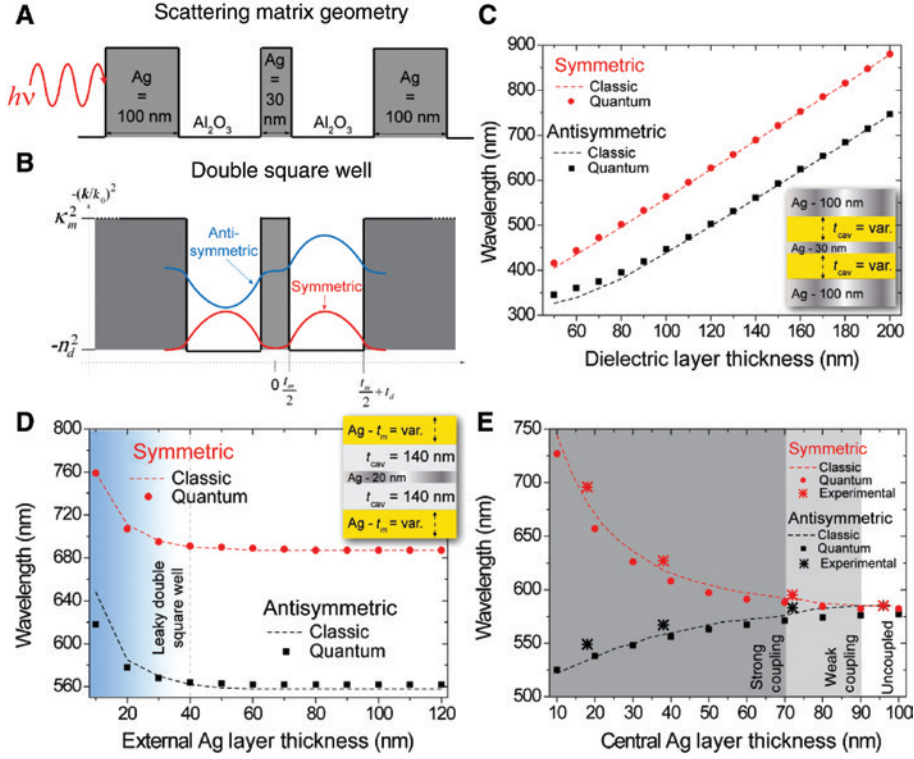
Figure 4: Quantum mechanical model of the MIMIM cavity.
(A) Structure of a MIMIM with thick external metal layers as used for SMM calculations. (B) Double quantum well that is the quantum mechanical analogue of the MIMIM structure. The y-scale for the optical potential is $-(k/k_0)^2$, and the origin of the x-axis is chosen in the middle of the central barrier. The barrier height of the potential for the photons induced by the metal layers is given by the square of the imaginary part of the refractive index κ_m^2, whereas the potential in the dielectric is at $-n_\mathrm{d}^2$. (C and D) Resonance frequencies calculated with the quantum approach (markers) and numerical SMM simulations (dashed lines) for different thickness of the dielectric layers (C) and the external Ag layers. (E) Experimental (large markers), quantum calculated (small markers), and SMM simulated resonance wavelengths of MIMIM structures with different central metal layer thicknesses. The mode splitting can be tuned from uncoupled resonators, through weak coupling, into the strong coupling regime. The largest experimental mode splitting is 477 meV for a central metal layer thickness of 18 nm, which is among the highest values reported in the literature [12, 13, 44–52].

well in quantum mechanics that allows to resolve this problem. Furthermore, this treatment leads to analytical expressions for the cavity resonances that describe the MIMIM with high accuracy and provides a more intuitive physical insight to such a complex photonic system. The geometry for the SMM calculation for MIMIM with thick external metal layers is shown in Figure 4A. The corresponding double quantum well with infinitely thick external barriers is depicted in Figure 4B together with the symmetric and antisymmetric eigenmodes that such a system sustains. In Ref. [5], we demonstrated that the square of the imaginary part of the dielectric permittivity of the metal, κ, can be seen as the optical equivalent of the potential that defines the barrier height. The semiclassical treatment for the MIM cavity that we developed on this basis can be straightforwardly extended to the MIMIM structure, thus allowing to find the dispersion relations that define the resonant modes:

$$\tanh\left(k_0\kappa_\mathrm{m}\frac{t_\mathrm{cm}}{2}\right) = \frac{\kappa_\mathrm{m}}{n_\mathrm{d}}\tan\left[-k_0 n_\mathrm{d}\left(\frac{1}{k_0\kappa_\mathrm{m}}+t_\mathrm{d}\right)\right] \tag{2}$$

$$-\coth\left(k_0\kappa_\mathrm{m}\frac{t_\mathrm{cm}}{2}\right) = \frac{\kappa_\mathrm{m}}{n_\mathrm{d}}\tan\left[-k_0 n_\mathrm{d}\left(\frac{1}{k_0\kappa_\mathrm{m}}+t_\mathrm{d}\right)\right] \tag{3}$$

The details on the derivation of these relations are reported in the SI. Figure 4C shows the resonance frequencies obtained by solving Eqs. (2) and (3) for different dielectric layer thicknesses, in the case of external metal layers with 100 nm thickness. The comparison to the numerical electromagnetic (SMM) simulations shows excellent agreement. As we consider illumination of the structures from the top, i.e. through the metal layers, MIMIM structures with thinner Ag layers are of large practical interest. In this case, the tunneling of the photon through the barrier has to be taken into account by an additional phase factor of

$-\exp(-2k_0\kappa_m t_m)$. Then, the dispersion relation for a "leaky" MIMIM structure is

$$\tanh\left(k_0\kappa_m \frac{t_{cm}}{2}\right) = \frac{\kappa_m}{n_d}\tan\left(-k_0 n_d\left(\frac{1}{k_0\kappa_m}+t_d\right)\right.$$
$$\left. -\exp(-2k_0\kappa_m t_m)\right) \tag{4}$$

$$-\coth\left(k_0\kappa_m \frac{t_{cm}}{2}\right) = \frac{\kappa_m}{n_d}\tan\left(-k_0 n_d\left(\frac{1}{k_0\kappa_m}+t_d\right)\right.$$
$$\left. -\exp(-2k_0\kappa_m t_m)\right) \tag{5}$$

The resulting resonance frequencies for the symmetric and asymmetric modes are plotted in Figure 4D as a function of the thickness of the external Ag layers. Here, the thickness of the dielectric layers was fixed at 140 nm, and the central metal layer was 20 nm thick. We clearly observe a decrease in resonance frequency when the thickness of the external layers is smaller than 40 nm, which identifies the leaky regime, where the additional phase correction in Eqs. (4) and (5) is necessary. Again, a very good agreement with the numerical (SMM) modeling, as shown by dashed lines, is obtained. The electric and magnetic field profiles of the resonant modes in such a leaky MIMIM structure, as calculated by finite-element method simulations (COMSOL Multiphysics), are reported in Figure S2 in the SI. From the experimental data in Figure 2C, we already saw that the coupling strength of the modes is determined by the thickness of the central metal layer. The double quantum well model of the MIMIM illustrates this coupling as resonant tunneling of the photons between the two wells, and Figure 4E shows that also the asymmetric mode splitting is well described by the quantum mechanical treatment (as depicted as small symbols). The experimental and theoretical data in Figure 4E demonstrate that the coupling in the MIMIM cavity can be tuned through the entire range, from uncoupled, to weakly coupled and strongly coupled by acting on the thickness of the central layer. The strong coupling regime is reached if $\dfrac{4g^2}{\gamma_{MIM_1}\cdot\gamma_{MIM_2}}>1$, where g is the coupling constant $\left(g=\dfrac{\hbar\Omega}{2}\right)$, with $\hbar\Omega$ being the mode splitting in meV, and γ_{MIM_1} and γ_{MIM_2} are the linewidths of the uncoupled modes. We note that, for an infinitely thin central metal layer, the resonances approach the symmetric and asymmetric modes in a MIM system and that, for a very thick central metal layer, the bottom cavity is shielded by the top one, which leads to the optical response of a

MIM superabsorber [5, 53]. Figure 4 demonstrates that the semiclassical approach, treating the MIMIM as a double quantum well for photons, allows for accurate analytical calculation of the resonance energies and provides physical insight in the mode coupling and mode confinement as related to photon tunneling through the metal barriers.

3 Conclusions

We demonstrated that the mode coupling in MIMIM double cavities allows to tailor their optical resonances in the visible spectral range. Spectroscopic ellipsometry identified the cavity resonances as ENZ modes, and a quantum mechanical view elucidated that their hybridization can be seen as resonant tunneling of photons through the central metal layer. Within the quantum mechanical treatment, we were able to describe the dependence of the spectral position of the ENZ modes on all geometrical and optical parameters of the constituent materials. MIMIM cavities can be a versatile platform for basic studies and practical applications where multiple tunable high-quality photonic resonances are needed.

4 Materials and methods

4.1 Fabrication and characterization of MIMIM structures

A multistep process was followed to fabricate the MIMIM structures consisting of deposition of (i) the metal (Ag) and (ii) the dielectric (Al_2O_3) stacked layers. (i) The Ag layer was deposited via electron beam-induced thermal evaporation (Kurt J. Lesker PVD 75) on a glass substrate followed by (ii) the deposition of 10 nm Al_2O_3 inside the same system, thus preventing Ag from oxidation. The remaining Al_2O_3 was deposited via atomic layer deposition (ALD; FlexAl from Oxford Instruments) using a thermal deposition process with a stage temperature of 110°C, obtaining an alumina deposition rate of 0.09 nm/cycle. Trimethylaluminate (TMA) and H_2O were used as precursors. A heating step of 300 s was performed before starting the ALD cycles. Each ALD cycle consisted of a H_2O/purge/TMA/purge sequence with a pulse durations of 0.075/6/0.033/2 s, respectively.

Spectroscopic ellipsometry was used to characterize the optical response and thickness of all the samples as well as a versatile experimental tool for the detection of polarized scattering parameters (reflectance, transmittance, and absorbance). A Vertical Vase ellipsometer by

Woollam was used in the range from 300 to 900 nm. Spectroscopic analysis has been carried out at three different angles (50°, 60°, and 70°) with a step of 3 nm. For both the experiments and spectroscopic characterization, a resolution of 3 nm was selected and all spectra have been normalized to the intensity of the Xe lamp.

4.2 Modeling and simulations

Finite-element method-based full-field simulations have been carried out by means of COMSOL Multiphysics. As boundary conditions, appropriately swept-meshed perfectly matched layers have been imposed, whereas the nanometric layers constituting the MIMIM have been meshed with a free triangular texture in which the maximum element size is 2 nm. Illumination is provided by a plane wave impinging at 40° via a classic internal port excitation, adjacent to the upper perfectly matched layer domain. Dielectric permittivities of all the selected materials were taken from experimentally measured data. SMM simulations have been conducted by means of a customized MATLAB code.

References

[1] Shaltout AM, Kim J, Boltasseva A, Shalaev VM, Kildishev AV. Ultrathin and multicolour optical cavities with embedded metasurfaces. Nat Commun 2018;9:2673–80.

[2] Ee H-S, Park H-G, Kim S-K. Design of high *Q*-factor metallic nanocavities using plasmonic bandgaps. Appl Opt 2016;55:1029–33.

[3] Chorsi HT, Lee Y, Alù A, Zhang JXJ. Tunable plasmonic substrates with ultrahigh *Q*-factor resonances. Sci Rep 2017;7:1–9.

[4] Weimer WA, Dyer MJ. Tunable surface plasmon resonance silver films. Appl Phys Lett 2001;79:3164–6.

[5] Caligiuri V, Palei M, Imran M, Manna L, Krahne R. Planar double-epsilon-near-zero cavities for spontaneous emission and Purcell effect enhancement. ACS Photonics 2018;5:2287–94.

[6] Dionne JA, Lezec HJ, Atwater HA. Highly confined photon transport in subwavelength metallic slot waveguides. Nano Lett 2006;6:1928–32.

[7] Caligiuri V, Palei M, Biffi G, Artyukhin S, Krahne R. A semi-classical view on epsilon-near-zero resonant tunneling modes in metal/insulator/metal nanocavities. Nano Lett 2019. DOI: 10.1021/acs.nanolett.9b00564.

[8] Alaeian H, Dionne JA. Non-Hermitian nanophotonic and plasmonic waveguides. Phys Rev B Condens Matter Mater Phys 2014;89:1–9.

[9] Savasta S, Saija R, Ridolfo A, Di Stefano O, Denti P, Borghese F. Nanopolaritons: vacuum Rabi splitting with a single quantum dot in the center of a dimer nanoantenna. ACS Nano 2010;4:6369–76.

[10] Novotny L. Strong coupling, energy splitting, and level crossings: a classical perspective. Am J Phys 2010;78:1199–202.

[11] Luk'yanchuk B, Zheludev NI, Maier SA, et al. The Fano resonance in plasmonic nanostructures and metamaterials. Nat Mater 2010;9:707–15.

[12] Liu Z, Li J, Liu Z, et al. Fano resonance Rabi splitting of surface plasmons. Sci Rep 2017;7:8010.

[13] Balci S, Karademir E, Kocabas C. Strong coupling between localized and propagating plasmon polaritons. Opt Lett 2015;40:3177–80.

[14] Lezec HJ, Dionne JA, Atwater HA. Negative refraction at visible frequencies. Science 2007;316:430–2.

[15] Dionne JA, Sweatlock LA, Atwater HA, Polman A. Planar metal plasmon waveguides: frequency-dependent dispersion, propagation, localization, and loss beyond the free electron model. Phys Rev B Condens Matter Mater Phys 2005;72:075405.

[16] Dionne JA, Sweatlock LA, Atwater HA, Polman A. Plasmon slot waveguides: towards chip-scale propagation with subwavelength-scale localization. Phys Rev B Condens Matter Mater Phys 2006;73:035407.

[17] Mrabti A, Lévêque G, Akjouj A, et al. Elastoplasmonic interaction in metal-insulator-metal localized surface plasmon systems. Phys Rev B 2016;94:075405.

[18] Kim J, Carnemolla EG, DeVault C, et al. Ferrera M, Boltasseva A. Dynamic control of nanocavities with tunable metal oxides. Nano Lett 2018;18:740–6.

[19] Schaffernak G, Krug MK, Belitsch M, et al. Plasmonic dispersion relations and intensity enhancement of metal-insulator-metal nanodisks. ACS Photonics 2018;5:4823–7.

[20] Hackett LP, Ameen A, Li W, Dar FK, Goddard LL, Liu GL. Spectrometer-free plasmonic biosensing with metal-insulator-metal nanocup arrays. ACS Sensors 2018;3:290–8.

[21] Verre R, Yang ZJ, Shegai T, Käll M. Optical magnetism and plasmonic Fano resonances in metal-insulator-metal oligomers. Nano Lett 2015;15:1952–8.

[22] Tagliabue G, Poulikakos D, Eghlidi H. Three-dimensional concentration of light in deeply sub-wavelength, laterally tapered gap-plasmon nanocavities. Appl Phys Lett 2016;108:221108.

[23] Limonov MF, Rybin MV, Poddubny AN, Kivshar YS. Fano resonances in photonics. Nat Photonics 2017;11:543–54.

[24] Meng ZM, Qin F. Realizing prominent Fano resonances in metal-insulator-metal plasmonic Bragg gratings side-coupled with plasmonic nanocavities. Plasmonics 2018;13:1–8.

[25] Moon K, Lee T-W, Lee Y, Kwon S-H. A metal-insulator-metal deep subwavelength cavity based on cutoff frequency modulation. Appl Sci 2017;7:86.

[26] Ferraro A, Zografopoulos DC, Caputo R, Beccherelli R. Broad- and narrow-line terahertz filtering in frequency-selective surfaces patterned on thin low-loss polymer substrates. IEEE J Sel Top Quantum Electron 2017;23:1–8.

[27] Caligiuri V, Dhama R, Sreekanth KV, Strangi G, De Luca A. Dielectric singularity in hyperbolic metamaterials: the inversion point of coexisting anisotropies. Sci Rep 2016;6:20002.

[28] Maier SA. Plasmonics: fundamentals and applications. New York: Springer, 2007.

[29] Caligiuri V, Pezzi L, Veltri A, De Luca A. Resonant gain singularities in 1D and 3D metal-dielectric multilayered nanostructures. ACS Nano 2017;11:1012–25.

[30] Castaldi G, Galdi V, Alù A, Engheta N. Nonlocal transformation optics. Phys Rev Lett 2012;108:063902.

[31] Savoia S, Castaldi G, Galdi V, Alù A, Engheta N. Tunneling of obliquely incident waves through PT-symmetric epsilon-near-zero bilayers. Phys Rev B Condens Matter Mater Phys 2014;89:085105.

[32] Javani MH, Stockman MI. Real and imaginary properties of epsilon-near-zero materials. Phys Rev Lett 2016;117:107404–10.

[33] Engheta N. Pursuing near-zero response. Science 2013;340:286–8.

[34] Alù A, Silveirinha MG, Salandrino A, Engheta N. Epsilon-near-zero metamaterials and electromagnetic sources: tailoring the radiation phase pattern. Phys Rev B Condens Matter Mater Phys 2007;75:155410–23.

[35] Ferrell RA, Stern EA. Plasma resonance in the electrodynamics of metal films. Am J Phys 1962;30:810–2.

[36] Ferrell RA. Predicted radiation of plasma oscillations in metal films. Phys Rev 1958;111:1214–22.

[37] Berreman DW. Infrared absorption at longitudinal optic frequency in cubic crystal films. Phys Rev 1963;130:2193–8.

[38] Newman W, Cortes CL, Atkinson J, Pramanik S, DeCorby RG, Jacob Z. Ferrell-Berreman modes in plasmonic epsilon-near-zero media. ACS Photonics 2014;2:2–7.

[39] Li Z, Butun S, Aydin K. Large-area, lithography-free super absorbers and color filters at visible frequencies using ultrathin metallic films. ACS Photonics 2015;2:183–8.

[40] Caligiuri V, Lento R, Ricciardi L, et al. Environmental control of the topological transition in metal/photoemissive-blend metamaterials. Adv Opt Mater 2018;6:1–8.

[41] Belov PA, Marqués R, Maslovski SI, et al. Strong spatial dispersion in wire media in the very large wavelength limit. Phys Rev B 2003;67:113103.

[42] Born M, Wolf E. Principles of optics electromagnetic theory of propagation, interference and diffraction of light. Oxford, UK: Pergamon Press, 1980.

[43] Caligiuri V, De Luca A. Metal-semiconductor-oxide extreme hyperbolic metamaterials for selectable canalization wavelength. J Phys D Appl Phys 2016;49:08LT01.

[44] Törmä P, Barnes WL. Strong coupling between surface plasmon polaritons and emitters: a review. Recent citations. Rep Prog Phys 2015;78:013901–35.

[45] Prodan E, Radloff C, Halas NJ, Nordlander P. A hybridization model for the plasmon response of complex nanostructures. Science 2003;302:419–22.

[46] Melnikau D, Esteban R, Savateeva D, et al. Rabi splitting in photoluminescence spectra of hybrid systems of gold nanorods and J-aggregates. J Phys Chem Lett 2016;7:354–62.

[47] Yoshle T, Scherer A, Hendrickson J, et al. Vacuum Rabi splitting with a single quantum dot in a photonic crystal nanocavity. Nature 2004;432:200–3.

[48] George J, Wang S, Chervy T, et al. Ultra-strong coupling of molecular materials: spectroscopy and dynamics. Faraday Discuss 2015;178:281–94.

[49] Ameling R, Giessen H. Microcavity plasmonics: strong coupling of photonic cavities and plasmons. Laser Photonics Rev 2013;7:141–69.

[50] Tsargorodska A, Cartron ML, Vasilev C, et al. Strong coupling of localized surface plasmons to excitons in light-harvesting complexes. Nano Lett 2016;16:6850–6.

[51] Peter E, Senellart P, Martrou D, et al. Exciton-photon strong-coupling regime for a single quantum dot embedded in a microcavity. Phys Rev Lett 2005;95:067401.

[52] Reithmaier JP, Sęk G, Löffler A, et al. Strong coupling in a single quantum dot-semiconductor microcavity system. Nature 2004;432:197–200.

[53] Li L, Wang W, Luk TS, Yang X, Gao J. Enhanced quantum dot spontaneous emission with multilayer metamaterial nanostructures. ACS Photonics 2017;4:501–8.